NTFA versus analytical estimates: theoretical comparison and benchmarking for particulate composites with constituents having a linear viscoelastic behavior

R. Largenton[a], J.-C. Michel[b], R. Masson[c]

a. EDF-R&D, MMC, CEA Cadarache, Bât. 151, 13108 St Paul lez Durance Cedex, rodrigue.largenton@edf.fr
b. Aix Marseille Univ, CNRS, Centrale Marseille, LMA UMR 7031, Marseille, michel@lma.cnrs-mrs.fr
c. CEA Cadarache, Bât. 151, 13108 St Paul lez Durance Cedex, renaud.masson@cea.fr

Résumé :

Cette étude présente et compare deux modélisations micromécaniques d'un matériau hétérogène : un matériau composite triphasé composé de deux phases inclusionnaires dispersées dans une phase matrice. Les phases ont un comportement viscoélastique linéaire avec gonflement. Dans un premier temps, la première approche est présentée: modèle analytique nommé MTI. Puis, la seconde approche par réduction de modèle est exposée : modèle NTFA. Dans un troisième temps, les deux approches sont comparées théoriquement et les précisions des deux approches sont évaluées par comparaison à des simulations en champs complets sur différents essais. La comparaison théorique souligne une grande analogie entre les deux approches mais également des différences clés. Les prédictions des deux modèles sont excellentes par rapport aux calculs en champs complets et ce pour différentes conditions de chargements.

Abstract:

This study presents and compares two micromechanical modelings of a heterogeneous material: a three-phase particulate composite material with two inclusion phases dispersed in a contiguous matrix. The phases have a linear viscoelastic behavior with swelling. First of all, the first approach is introduced: analytical model named MTI. Then the model-reduction approach is developed: NTFA model. Third, a theoretical comparison between these two approaches is presented while their accuracies are assessed by comparison with full-field simulations. The theoretical comparison realized in this paper underlines a huge analogy between the two approaches, but also some key differences. The predictions of both models are in excellent agreement with full-field simulations for various loading conditions.

Keywords: Micromechanics, Correspondence principle, Model reduction, Linear, Composite, Viscoelasticity, Swelling, Theoretical comparison, Benchmarking

1 Introduction

Constitutive relations of solid materials are usually formulated at the engineering, or macroscopic, scale. However, as the loadings become more complex, an accurate description of their response requires the introduction of more internal variables, whose physical meaning is not always clear and for which calibration of more material parameters is needed. Micromechanical approaches provide an alternative to this phenomenological formulation of macroscopic constitutive relations, based on the observation that all solid materials are heterogeneous at a small enough scale. Micromechanical models for viscoelastic composites fall, roughly speaking, into one of three following categories:

1. *Analytical models.*
2. *Full-field simulations*.
3. *Reduced-order models.*

This study presents and compares two micromechanical modelings of an heterogeneous material already considered in [2]: a three-phase particulate composite material with two inclusion phases dispersed in a contiguous matrix. The phases have a linear viscoelastic behavior with swelling. First, the analytical approach, named MTI model [1, 6], is introduced and then the model-reduction approach named NTFA model [2, 5]. Third, a theoretical comparison between the two approaches is presented and their accuracies are assessed by comparison with full-field simulations on different tests.

2 Composite and relations for the individual constituents

Three-phase particulate composite will serve to illustrate the theory developed in this study. It is a material with three distinct phases: a connected matrix containing two spherical inclusion phases dispersed in this one [2]. The first inclusion phase, named Pu clusters and shown in red in Figure 1, has a volume fraction of 15%. The diameter of Pu clusters varies in the range $[10\mu\text{m}, 70\mu\text{m}]$. The second inclusion phase, named U clusters and shown in blue in Figure 1, has a volume fraction of 25%. The diameter of the U clusters is equal to 30μm.

For this composite material, the total strain at a material point $\boldsymbol{x}$ in each of the phases can be decomposed into three contributions:

$$\boldsymbol{\varepsilon}(\boldsymbol{x},t) = \boldsymbol{\varepsilon}_{\mathsf{e}}(\boldsymbol{x},t) + \boldsymbol{\varepsilon}_{\mathsf{v}}(\boldsymbol{x},t) + \boldsymbol{\varepsilon}_{\mathsf{s}}(\boldsymbol{x},t), \tag{1}$$

where $\boldsymbol{\varepsilon}_{\mathsf{e}}$ is the elastic strain, $\boldsymbol{\varepsilon}_{\mathsf{v}}$ is the viscous strain and $\boldsymbol{\varepsilon}_{\mathsf{s}}$ is an eigenstrain of swelling. The elastic strain is related to the stress $\boldsymbol{\sigma}$ by the elastic compliance $\boldsymbol{M}^{(r)}$ (inverse of the elastic stiffness $\boldsymbol{L}^{(r)}$):

$$\boldsymbol{\varepsilon}_{\mathsf{e}}(\boldsymbol{x},t) = \boldsymbol{M}^{(r)} : \boldsymbol{\sigma}(\boldsymbol{x},t), \quad \boldsymbol{x} \text{ in phase } r. \tag{2}$$

The creep strain is purely deviatoric and depends on the stress $\boldsymbol{\sigma}$ through a linear relation involving a scalar shear viscosity $G_{\mathsf{v}}^{(r)}$ which is uniform in phase r:

$$\dot{\boldsymbol{\varepsilon}}_{\mathsf{v}}(\boldsymbol{x},t) = \frac{1}{2G_{\mathsf{v}}^{(r)}}\boldsymbol{s}(\boldsymbol{x},t) \quad \text{in phase } r, \tag{3}$$

where $\boldsymbol{s}$ is the stress deviator. The values of $G_{\mathsf{V}}^{(r)}$ in each phase are given in Table 1. Moreover, the elasticity of the phases is assumed to be isotropic with the same moduli in each phase: see Table 1. The swelling strain is isotropic, uniform per phase and is a linear function of time:

$$\boldsymbol{\varepsilon}_{\mathsf{S}}(\boldsymbol{x},t) = \varepsilon_{\mathsf{S}}^{(r)}(t)\,\boldsymbol{i} = \dot{\varepsilon}_{\mathsf{S}}^{(r)} t\,\boldsymbol{i}, \quad \boldsymbol{x} \text{ in phase } r, \tag{4}$$

where $\boldsymbol{i}$ is the second-order identity tensor and $\dot{\varepsilon}_{\mathsf{S}}^{(r)}(t)$ is the swelling rate in each phase: their values in each phase are given in Table 1.

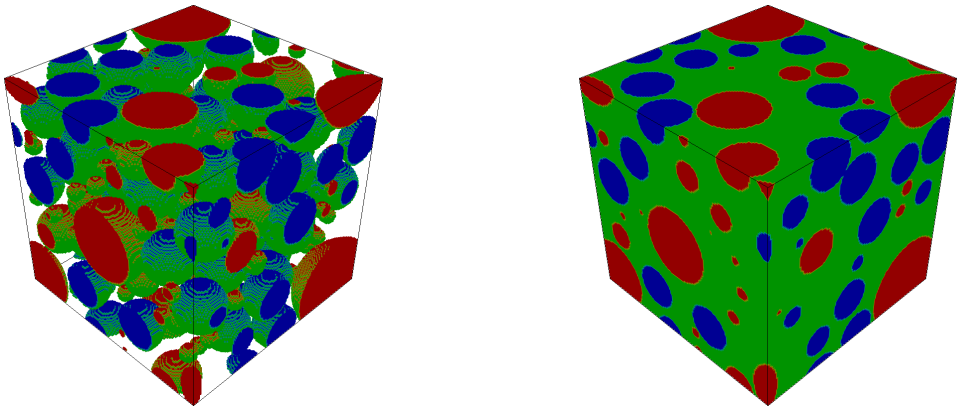

(a) (b)

Figure 1: Three-dimensional volume element of the three-phase particulate composite. (**a**) Inclusions only - Pu clusters (in red), U clusters (blue). (**b**) Entire volume element - matrix (green).

Phase	E (GPa)	ν (-)	$G_{\mathsf{V}}^{(r)}$ (GPa.s)	$\dot{\varepsilon}_{\mathsf{S}}^{(r)}$ (s^{-1})	Volume Fraction $(-)$
Matrix (r=1)	200	0.3	52.94	$7.00E-05$	0.60
Pu clusters (r=2)	200	0.3	21.43	$2.10E-03$	0.15
U clusters (r=3)	200	0.3	158.83	$2.84E-05$	0.25

Table 1: Material data for the individual constituents.

It should be noticed that the contrast in the swelling strain between the Pu clusters and the matrix used in the numerical simulations is artificially larger than in reality: 30 instead of 3. This is done on purpose to magnify the effect of the mismatch between the phases. Moreover, $G_{\mathsf{V}}^{(r)}$ are artificially smaller than in reality to raise the creep rates in the phases and in order to reduce the computation time.

3 Local problem

For this three-phase particulate composite, V is the chosen volume element. The response of the volume element V to a mechanical loading is simulated numerically on a time interval $[0,t]$ by solving the equilibrium and compatibility equations together with the constitutive relations of the individual phases

and appropriate boundary conditions:

$$\begin{cases} \text{div}(\boldsymbol{\sigma}(\boldsymbol{x},t)) = 0, \quad \boldsymbol{\varepsilon}(\boldsymbol{x},t) = \frac{1}{2}\left(\boldsymbol{\nabla}\boldsymbol{u}(\boldsymbol{x},t) + \boldsymbol{\nabla}\boldsymbol{u}^{\mathsf{T}}(\boldsymbol{x},t)\right), \\ \boldsymbol{\sigma}(\boldsymbol{x},t) = \boldsymbol{L}(\boldsymbol{x}) : (\boldsymbol{\varepsilon}(\boldsymbol{x},t) - \boldsymbol{\varepsilon}_{\mathsf{s}}(\boldsymbol{x},t) - \boldsymbol{\varepsilon}_{\mathsf{v}}(\boldsymbol{x},t)) \ , \\ \boldsymbol{\varepsilon}_{\mathsf{s}}(\boldsymbol{x},t) = \sum_{r=1}^{N} \chi^{(r)}(\boldsymbol{x}) \ \varepsilon_{\mathsf{s}}^{(r)}(t)\, \boldsymbol{i} \ , \ \dot{\boldsymbol{\varepsilon}}_{\mathsf{v}}(\boldsymbol{x},t) = \sum_{r=1}^{N} \chi^{(r)}(\boldsymbol{x}) \frac{\boldsymbol{s}(\boldsymbol{x},t)}{2G_{\mathsf{v}}^{(r)}} \\ \boldsymbol{u}(\boldsymbol{x},t) = \overline{\boldsymbol{\varepsilon}}(t).\boldsymbol{x} + \boldsymbol{u}^{*}(\boldsymbol{x},t) \ , \ \boldsymbol{u}^{*}(\boldsymbol{x},t) \ \ \# \text{ and } \boldsymbol{\sigma}(\boldsymbol{x},t).\boldsymbol{n}(\boldsymbol{x}) \ \ \text{-\#} \ , \end{cases} \tag{5}$$

where $\chi^{(r)}(\boldsymbol{x})$ is the characteristic function of phase r and $c^{(r)}$ its volume fraction. Periodic boundary conditions are assumed on the boundary of the volume element and this choice is reflected by the periodicity of $\boldsymbol{u}^{*}$ (notation #) and anti-periodicity of $\boldsymbol{\sigma}.\boldsymbol{n}$ (notation -#) on the boundary of V. The loading is specified by imposing the macroscopic strain path $\overline{\boldsymbol{\varepsilon}}(t)$ and the swelling history $\varepsilon_{\mathsf{s}}^{(r)}(t)$ in each phase.

The effective (or homogenized) constitutive relations relate the overall stress $\overline{\boldsymbol{\sigma}}(t)$ defined as the average of the local stress field

$$\overline{\boldsymbol{\sigma}}(t) = \langle \boldsymbol{\sigma}(\boldsymbol{x},t) \rangle = \frac{1}{|V|} \int_{V} \boldsymbol{\sigma}(\boldsymbol{x},t)\, d\boldsymbol{x},$$

to the history of the overall strain $\overline{\boldsymbol{\varepsilon}}$ and of the swelling strains $\varepsilon_{\mathsf{s}}^{(r)}$. *NB: later in this paper the spatial averaging over V and $V^{(r)}$ are denoted by $\langle . \rangle$ and $\langle . \rangle^{(r)}$ respectively.*

4 Analytical model - MTI

For non aging linear viscoelastic composites, the earlier analytical models use the Laplace transform: the problem is reduced to finding the effective properties of elastic composites with moduli depending on the Laplace parameter. [1, 6] showed that for specific microstructures, two-phase or three-phase particulate composites whose overall elastic properties are given by one of the Hashin-Shtrikman bounds, the relaxation spectrum of the composites remains discrete. This implies that the overall constitutive relations of such composites can be alternatively written with a *finite* number of internal variables.

In this section we present briefly the model developped by [1, 6], model named MTI (*Mori-Tanaka Incremental*), and we apply it to our case of interest. The N phases (matrix $r = 1$, Pu $r = 2$ and U clusters $r = 3$) obey to an isotropic maxwellian behaviour and the exact local problem presented in (5) with decomposition (4) can be re-written as a system of differential equations:

$$\begin{cases} \dot{\varepsilon}^{m}(\boldsymbol{x},t) = \dfrac{1}{3K}\dot{\sigma}^{m}(\boldsymbol{x},t) + \dot{\varepsilon}_{s}^{m}(\boldsymbol{x},t), \\ \dot{\boldsymbol{e}}(\boldsymbol{x},t) = \dfrac{1}{2G}\dot{\boldsymbol{s}}(\boldsymbol{x},t) + \dot{\boldsymbol{e}}_{\mathsf{v}}(\boldsymbol{x},t), \\ \dot{\varepsilon}_{s}^{m}(\boldsymbol{x},t) = \sum_{r=1}^{N} \dot{\varepsilon}_{s}^{m(r)}(\boldsymbol{x},t)\chi^{(r)}(\boldsymbol{x}), \\ \dot{\boldsymbol{e}}_{\mathsf{v}}(\boldsymbol{x},t) = \sum_{r=1}^{N} \dfrac{1}{2G_{\mathsf{v}}^{(r)}} \boldsymbol{s}(\boldsymbol{x},t)\chi^{(r)}(\boldsymbol{x}), \end{cases} \tag{6}$$

with K and G the elastic bulk and shear moduli (elastic moduli assumed to be the same in each phase), $\sigma_{\mathsf{m}} = \frac{1}{3}Tr(\boldsymbol{\sigma})$, $\dot{\varepsilon}^{m}$ and $\dot{\boldsymbol{e}}_{\mathsf{v}}$ the hydrostatic and deviatoric strain rates and $\dot{\varepsilon}_{s}^{m}$ the swelling rate.

As mentioned previously to derive the effective behavior of linear viscoelastic heterogeneous media, the Laplace–Carson transform and the correspondence principle [3] are classically used. This functional transform allows to define a symbolic linear elastic composite in the Laplace domain. Linear homogenization models are then applied to this fictitious elastic body to derive its effective properties. In [1] overall elastic properties in the Laplace–Carson domain are given by one of the Hashin-Shtrikman bounds. The viscoelastic effective properties (for instance the effective relaxation function) are then deduced by the inversion of the Laplace–Carson transform. For more detailed information related to these developments, the reader can refer to [1]. As the *Hashin-Shtrikman* chosen bound identifies to the classical *Mori-Tanaka (1973)* estimate, this model is called *Mori-Tanaka incremental*: *incremental* being related to the internal variable formulation. In our case of interest, we present only the effective results of this model and obviously the internal variable formulation:

$$\begin{cases} \overline{\sigma}^m = 3K\left(\overline{\varepsilon}^m(t) - \overline{\varepsilon}_s^m\right) \ , \\ \\ \overline{\boldsymbol{s}} = 2G\left(\overline{\boldsymbol{e}}(t) - \sum_{i=1}^{N^d_{(HS)}} \boldsymbol{\alpha}_i(t)\right) \ , \\ \\ \text{with} \quad \dot{\boldsymbol{\alpha}}_i(t) + \dfrac{1}{\overline{\tau}^d_{(HS)i}}\boldsymbol{\alpha}_i(t) = \dfrac{1}{\overline{\tau}^d_{(HS)i}}\dfrac{\mu_{\overline{\tau}^d_{(HS)i}}}{G}\overline{\boldsymbol{e}}(t) \quad , \quad 1 \leq i \leq N^d_{(HS)} \ , \ \boldsymbol{\alpha}_i(0) = \mathbf{0}. \end{cases} \tag{7}$$

with $\overline{\sigma}^m$ and $\overline{\boldsymbol{s}}$ the hydrostatic and deviatoric macroscopic stresses, $\overline{\varepsilon}^m(t)$ and $\overline{\boldsymbol{e}}$ the hydrostatic and deviatoric macroscopic strains, $N^d_{(HS)}$ the number of tensor deviatoric internal variables $\boldsymbol{\alpha}_i(t)$, $(\overline{\tau}^d_{(HS)i})$ the effective relaxation times and $(\mu_{\overline{\tau}^d_{(HS)i}})$ the associated magnitudes. The reader can refer to [1] for more details on these coefficients which are given as functions of the phase volume fractions and their elastic and viscous properties. $\overline{\varepsilon}_s^m$ is the effective swelling. As the compressibility of the composite is homogeneous the effective swelling $\overline{\varepsilon}_s^m$ is given by:

$$\overline{\varepsilon}_s^m = \sum_{r=1}^{N} c^{(r)} \varepsilon_{\mathsf{s}}^{(r)}(t). \tag{8}$$

As we can see the tensor internal variables $\boldsymbol{\alpha}_i(t)$ are solutions of first order linear differential equations. The average stress per phase are also given by first order linear differential equations. For more detailed information related to these evolution laws, the reader can refer to [1] and [6]. In this paper the theoretical comparison will be performed only on the effective evolution laws of the MTI and NTFA models (see section 6.1), that's why we describe only these effective evolutions laws.

5 Reduced order model - NTFA

Reduced models aim at achieving a compromise between the analytical approaches and Full-field simulations. They are based on numerical simulations at the microscopic scale (which can sometimes be replaced by analytical calculations) and on the other hand they deliver constitutive relations with a finite number of internal variables which can be used in macroscopic computations, at the expense of certain approximations which depend on the reduction method.

Among all the reduced order models there is the Nonuniform Transformation Field Analysis (NTFA) developed by [5]. The basic feature of the NTFA theory [5] is a decomposition of the viscous strain on

a set of a few, well-chosen, fields, called *modes*:

$$\boldsymbol{\varepsilon}_{\mathsf{v}}(\boldsymbol{x},t)=\sum_{k=1}^{M}\xi^{(k)}(t)\,\boldsymbol{\mu}^{(k)}(\boldsymbol{x}), \tag{9}$$

where

- in our case of interest the modes $\left(\boldsymbol{\mu}^{(k)}(\boldsymbol{x})\right)_{k=1,\dots,M}$ are incompressible tensorial fields (tr($\boldsymbol{\mu}^{k}$)=0) and orthogonal i.e. $\langle\boldsymbol{\mu}^{k}:\boldsymbol{\mu}^{l}\rangle=0$ si $k\neq l$. The choice of these modes is essential in the method and will be discussed in section 6.2.1. These modes have the same tensorial character as the internal variables $\boldsymbol{\varepsilon}_{\mathsf{v}}$.
- the $\left(\xi^{(k)}(t)\right)_{k=1,\dots,M}$'s are the generalized viscous strains associated with each mode for which evolution equations will be derived (see eq. (15)). Therefore, $\xi^{(k)}$ are the *scalar reduced internal variables*. To avoid a possible indeterminacy in the definition of the $\xi^{(k)}$, it is further assumed that the modes $\boldsymbol{\mu}^{(k)}$ are linearly independent fields.

Assume that the modes $\boldsymbol{\mu}^{(k)}(\boldsymbol{x})$ have been chosen: this choice is discussed in section 6.2.1. Then under the decomposition (9), it follows from the superposition principle used in (1) that the local strain field $\boldsymbol{\varepsilon}$ in the composite can be written as:

$$\boldsymbol{\varepsilon}(\boldsymbol{x},t)=\boldsymbol{A}(\boldsymbol{x}):\overline{\boldsymbol{\varepsilon}}(t)+\sum_{k=1}^{M}(\boldsymbol{D}*\boldsymbol{\mu}^{(k)})(\boldsymbol{x})\xi^{(k)}(t)+\sum_{r=1}^{N}(\boldsymbol{D}*\chi^{(r)}\boldsymbol{i})(\boldsymbol{x})\varepsilon_{\mathsf{s}}^{(r)}(t), \tag{10}$$

where $\boldsymbol{A}(\boldsymbol{x})$ is the elastic strain localization tensor, $\boldsymbol{D}(\boldsymbol{x},\boldsymbol{x}')$ is the nonlocal Green operator expressing the strain at point $\boldsymbol{x}$ resulting from a unit eigenstrain at point $\boldsymbol{x}'$ when the average strain vanishes and $*$ denotes the convolution in space. The elastic strain localization tensor $\boldsymbol{A}(\boldsymbol{x})$ and the influence tensors $\left(\boldsymbol{D}*\boldsymbol{\mu}^{(k)}\right)_{k=1,\dots,M}$, $\left(\boldsymbol{D}*\chi^{(r)}\boldsymbol{i}\right)_{r=1,\dots,N}$ can be computed once for all by solving $6+M+N$ linear elasticity problems (see [2]).

The corresponding stress field reads as:

$$\begin{gathered}\boldsymbol{\sigma}(\boldsymbol{x},t)=\boldsymbol{L}(\boldsymbol{x}):\boldsymbol{A}(\boldsymbol{x}):\overline{\boldsymbol{\varepsilon}}(t)+\sum_{k=1}^{M}\boldsymbol{\rho}^{(k)}(\boldsymbol{x})\xi^{(k)}(t)+\sum_{r=1}^{N}\boldsymbol{\eta}^{(r)}(\boldsymbol{x})\varepsilon_{\mathsf{s}}^{(r)}(t),\\ \boldsymbol{\rho}^{(k)}(\boldsymbol{x})=\boldsymbol{L}(\boldsymbol{x}):\left((\boldsymbol{D}*\boldsymbol{\mu}^{(k)})(\boldsymbol{x})-\boldsymbol{\mu}^{(k)}(\boldsymbol{x})\right),\quad \boldsymbol{\eta}^{(r)}(\boldsymbol{x})=\boldsymbol{L}(\boldsymbol{x}):\left((\boldsymbol{D}*\chi^{(r)}\boldsymbol{i})(\boldsymbol{x})-\chi^{(r)}(\boldsymbol{x})\boldsymbol{i}\right).\end{gathered} \tag{11}$$

The *reduced stress* associated with the k-th mode is defined as $\tau^{(k)}(t)=\langle\boldsymbol{\mu}^{(k)}(\boldsymbol{x}):\boldsymbol{\sigma}(\boldsymbol{x},t)\rangle$. Using eq. (11), the following relation is obtained:

$$\tau^{(k)}(t)=\boldsymbol{a}^{(k)}:\overline{\boldsymbol{\varepsilon}}(t)+\sum_{\ell=1}^{M}D^{(k\ell)}\xi^{(\ell)}(t)+\sum_{r=1}^{N}H^{(kr)}\varepsilon_{\mathsf{s}}^{(r)}(t), \tag{12}$$

where the influence tensors $\boldsymbol{a}^{(k)}$, $D^{(k\ell)}$ and $H^{(kr)}$ are given by:

$$\boldsymbol{a}^{(k)}=\langle\boldsymbol{\mu}^{(k)}:(\boldsymbol{L}:\boldsymbol{A})\rangle,\quad D^{(k\ell)}=\langle\boldsymbol{\mu}^{(k)}:\boldsymbol{\rho}^{(\ell)}\rangle,\quad H^{(kr)}=\langle\boldsymbol{\mu}^{(k)}:\boldsymbol{\eta}^{(r)}\rangle. \tag{13}$$

Using the constitutive equation (3) for the viscous strain-rate, the following relation between the $\tau^{(k)}$'s

and the $\xi^{(\ell)}$'s is obtained:

$$\dot{\xi}^{(\ell)}(t) = \sum_{m=1}^{M} W^{(\ell m)}(t)\tau^{(m)}(t) \quad . \tag{14}$$

where the incompressibility of the modes has been used, $\boldsymbol{W} = \boldsymbol{V}^{-1}$ and $V^{(k\ell)} = \langle 2G_{\mathsf{v}}\, \boldsymbol{\mu}^{(k)} : \boldsymbol{\mu}^{(\ell)} \rangle$.

Using eq. (12) and (14), a differential equation for the $\xi^{(k)}$'s is obtained:

$$\dot{\xi}^{(k)}(t) - \sum_{\ell=1}^{M}\sum_{m=1}^{M} W^{(k\ell)} D^{(\ell m)} \xi^{(m)}(t) = \sum_{\ell=1}^{M} W^{(k\ell)} \boldsymbol{a}^{(\ell)} : \overline{\boldsymbol{\varepsilon}}(t) + \sum_{\ell=1}^{M}\sum_{r=1}^{N} W^{(k\ell)} H^{(kr)} \varepsilon_{\mathsf{s}}^{(r)}(t) \ . \tag{15}$$

The local stress and strain field were expressed in terms of the state variables by means of relations (11) and (10). Finally the overall stress is obtained by averaging the local stress field:

$$\overline{\boldsymbol{\sigma}} = \widetilde{\boldsymbol{L}} : \overline{\boldsymbol{\varepsilon}} + \sum_{k=1}^{M} \langle \boldsymbol{\rho}^{(k)} \rangle \xi^{(k)} + \sum_{r=1}^{N} \langle \boldsymbol{\eta}^{(r)} \rangle \varepsilon_{\mathsf{s}}^{(r)} \ , \tag{16}$$

where $\widetilde{\boldsymbol{L}} = \langle \boldsymbol{L} : \boldsymbol{A} \rangle$ is the effective elastic stiffness tensor.

Finally and in our case of interest (the elasticity of the phases is assumed to be isotropic and homogeneous, the creep strain is purely deviatoric), we summarize below the effective results of NTFA model and more precisely the internal variable formulation:

$$\begin{cases} \overline{\sigma}^{m} = 3K\left(\overline{\varepsilon}^{m}(t) - \overline{\varepsilon}_{s}^{m}\right) \ , \\ \\ \overline{\boldsymbol{s}} = 2G(\overline{\boldsymbol{e}} - \sum_{k=1}^{M} \langle \boldsymbol{\mu}^{(k)} \rangle \xi^{(k)}) \ , \\ \\ \text{with:} \\ \\ \dot{\xi}^{(k)}(t) - \sum_{\ell=1}^{M}\sum_{m=1}^{M} W^{(k\ell)} D^{(\ell m)} \xi^{(m)}(t) = \sum_{\ell=1}^{M} W^{(k\ell)} \boldsymbol{a}^{(\ell)} : \overline{\boldsymbol{\varepsilon}}(t) + \sum_{\ell=1}^{M}\sum_{r=1}^{N} W^{(k\ell)} H^{(kr)} \varepsilon_{\mathsf{s}}^{(r)}(t) \\ \\ \text{and} \quad 1 \leq k \leq \text{M}. \end{cases} \tag{17}$$

M is the number of scalar intenal variables $\xi^{(k)}(t)$ and $\overline{\varepsilon}_{s}^{m}$ is given by eq. (8). The history of the internal state variables $(\xi^{(k)}(t))|_{k=1,\ldots,M}$ is completely determined by the resolution of this system of differential equations of order one.

6 Comparison of the MTI and NTFA models

In this section, we perform a comparison between the two approaches presented in sections 4 and 5. Subsection 6.1 is devoted to a theoretical comparison between the two approaches. In subsection 6.2 we assess the accuracy of both models (results for the overall response of the composite as well as for the average response of the phases) for three-phase particulate composites with constituents having linear viscoelastic behavior with swelling: the accuracies are assessed by comparison with full-field simulations on different tests.

6.1 Theoretical comparison of the models

In this section we consider an incompressible viscoelastic behavior without swelling in each phase (the elasticity of the phases is always assumed to be isotropic and homogeneous): the goal is to simplify the previous equations (see eq. (7) and (17)) and make them more readable. In this case of interest the equations (7) and (17) are given by the following ones:

$$\left\{\begin{array}{l} \textit{MTI approach:} \\ \\ \overline{\boldsymbol{s}} = 2G\left(\overline{\boldsymbol{e}}(t) - \sum_{i=1}^{N^d_{(HS)}} \boldsymbol{\alpha}_i(t)\right) \ , \\ \\ \text{with} \quad \dot{\boldsymbol{\alpha}}_i(t) + \dfrac{1}{\overline{\tau}^d_{(HS)i}}\boldsymbol{\alpha}_i(t) = \dfrac{1}{\overline{\tau}^d_{(HS)i}}\dfrac{\mu_{\overline{\tau}^d_{(HS)i}}}{G}\overline{\boldsymbol{e}}(t) \quad , \quad 1 \leq i \leq N^d_{(HS)} \ , \ \boldsymbol{\alpha}_i(0) = \mathbf{0}. \end{array}\right. \tag{18}$$

$$\left\{\begin{array}{l} \textit{NTFA approach:} \\ \\ \overline{\boldsymbol{s}} = 2G(\overline{\boldsymbol{e}} - \sum_{k=1}^{M}\langle\boldsymbol{\mu}^{(k)}\rangle\xi^{(k)}) \ , \\ \\ \text{with:} \\ \\ \dot{\xi}^{(k)}(t) - \sum_{\ell=1}^{M}\sum_{m=1}^{M}\left(\dfrac{1}{\tau^{(k\ell)}}\left[\langle\boldsymbol{\mu}^{(\ell)}(\boldsymbol{x}) : (\boldsymbol{D} * \boldsymbol{\mu}^{(m)})(\boldsymbol{x})\rangle - \delta^{(\ell m)}\right]\right)\xi^{(m)}(t) \\ \\ = \sum_{\ell=1}^{M}\left(\dfrac{1}{\tau^{(k\ell)}}\langle\boldsymbol{\mu}^{(\ell)}(\boldsymbol{x})\rangle\right) : \overline{\boldsymbol{e}}(t) \\ \\ \text{with} \quad \delta^{(\ell m)} \text{ Kronecker symbol,} \ \dfrac{1}{\tau^{(k\ell)}} = 2G\langle 2G_{\text{v}}\boldsymbol{\mu}^{(k)}(\boldsymbol{x}) : \boldsymbol{\mu}^{(\ell)}(\boldsymbol{x})\rangle^{-1} \quad \text{and} \quad 1 \leq k \leq \text{M}. \end{array}\right. \tag{19}$$

In this case the theoretical comparison between the effective evolution laws of MTI (see eq. (18)) and NTFA (see eq. (19)) models emphasizes a huge analogy. Indeed, we can notice that the $\boldsymbol{\alpha}_i(t)$ and $\xi^{(k)}(t)$'s solve a system of first order linear differential equations. Nevertheless, in the NTFA approach the internal variables are scalar and solve a system of coupled differential equations: in our case the numerical coupled term isn't negligible. Moreover the number of internal variables is different between the two models: 18 for the NTFA model and 30 for the MTI model (*NB :* $30 = 5N^d_{(HS)}$). Because of coupled term it's not easy to give a physical meaning to the internal variables of MTI model. However and in the future, it would be interesting to study if the relaxation times of MTI model would not be a new way to select the plastic modes of the NTFA approach.

6.2 Assessment of the models

6.2.1 Modes for NTFA model

The choice of the modes $\boldsymbol{\mu}^{(k)}$ plays a key-role in the efficiency of the method. There is no universal choice for these modes and they should rather be chosen according to the type of loading which the structure is likely to be subjected to. In this study the selected modes $\boldsymbol{\mu}^{(k)}$ are from the seven elementary

loadings and compute on the three-dimensional volume element shown in Figure 1: volume element having a total of 121 Pu clusters of different sizes and 57 U clusters (see [2] for more details on how this volume element was generated). The full-field simulations were performed using a code based on a fast Fourier transform method ([4]), the volume element shown in Figure 1 being discretized into 147^3 voxel To keep the loading conditions rather general, monotonic loadings of the volume element are simulated along given directions in the space of overall loadings, consisting of the overall stress $\overline{\boldsymbol{\sigma}}$ and of the swelling of the individual phases. In the present study, 6 purely mechanical loading paths have been defined by loading the volume element along 6 stress "directions" $\boldsymbol{\Sigma}_s^0$ with no swelling of the phases,

$$\overline{\boldsymbol{\sigma}}(t) = \overline{\sigma}(t)\boldsymbol{\Sigma}_s^0, \quad \varepsilon_{\mathsf{s}}^{(r)} = 0 \quad \text{in each phase,} \tag{20}$$

with

$$1 \leq s \leq 3: \quad \boldsymbol{\Sigma}_s^0 = \boldsymbol{e}_s \otimes \boldsymbol{e}_s,$$

and

$$4 \leq s \leq 6: \quad \boldsymbol{\Sigma}_s^0 = \frac{1}{2}\left(\boldsymbol{e}_i \otimes \boldsymbol{e}_j + \boldsymbol{e}_j \otimes \boldsymbol{e}_i\right), \quad s = 9 - i - j,$$

whereas the 7-th test correspond to pure swelling of the phases with no overall stress,

$$\boldsymbol{\Sigma}_7^0 = \mathbf{0}, \quad \dot{\varepsilon}_{\mathsf{s}}^{(r)} \text{ as in Table 1 for each phase.}$$

The first 3 stress directions correspond to uniaxial tension in the three different directions and the next 3 stress directions correspond to pure shear. Numerical simulations are carried out along these paths by increasing monotonically the strain in the direction of the applied stress (except for the loading case 7) up to 10 % deformation along the applied stress for the 6 first loading paths $\overline{\boldsymbol{\varepsilon}} : \boldsymbol{\Sigma}^0 = 10\%$, and up to $t = 10$ s for the 7-th loading path. For the first 6 loading paths the overall strain-rate is fixed $\dot{\overline{\boldsymbol{\varepsilon}}} : \boldsymbol{\Sigma}^0 = 10^{-2}s^{-1}$ so that 10 % deformation is attained in 10 s. The material data used in these simulations can be found in Table 1.

For each of these seven loading cases, 25 snapshots of the viscous strain field are stored every $0.4s$ seconds of the full-field simulation. The actual modes are then extracted from snapshots by means of the Karhunen–Loève transform procedure (for more details see [2]). After application of this procedure, a total of 18 modes were selected.

6.2.2 Performed tests

To compare the accuracy of MTI and NTFA models two tests have been performed:

Test 1. A relaxation test under uniaxial tension ($\overline{\sigma}_{ij} = 0$, except $\overline{\sigma}_{33}$). The overall strain in direction 3 is increased in 0.1 s from 0 to $\overline{\varepsilon}_{33} = 0.02$ and kept constant. The swelling rate in each phase is reported in Table 1.

Test 2. A non radial test involving a rotation of principal axes of the overall stress. The overall strain is imposed in the form

$$\overline{\boldsymbol{\varepsilon}}(t) = \varepsilon_0 \sin\omega t \left[\boldsymbol{e_1} \otimes \boldsymbol{e_1} - \frac{1}{2}\boldsymbol{e_2} \otimes \boldsymbol{e_2} - \frac{1}{2}\boldsymbol{e_3} \otimes \boldsymbol{e_3}\right] + \varepsilon_0(1 - cos(\omega t)) \left[\boldsymbol{e_1} \otimes_s \boldsymbol{e_2} + \boldsymbol{e_1} \otimes_s \boldsymbol{e_3}\right], \tag{21}$$

with $\varepsilon_0 = 0.1$, $\omega = \frac{\pi}{2}$. In this test, swelling is not activated. The response of the volume element is investigated for the first 5 cycles (20 s).

For these two tests, the predictions of the two approaches are compared with reference results obtained by full-field simulations using the material data in Table 1. To perform the full-field simulations we used the same discretized volume element involved to select modes (see Figure 1). The comparison is carried out for two types of information: the effective response of the composite and the average response of the phases.

6.2.3 Effective response of MTI and NTFA models

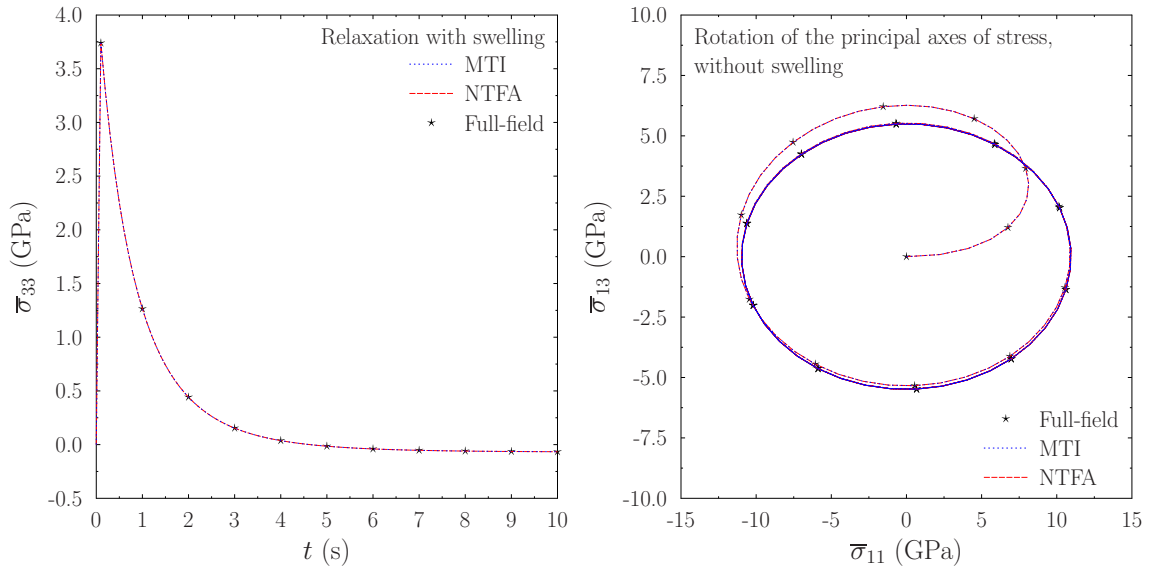

(a) (b)

Figure 2: Effective response. Comparison between full-field simulations (black symbols) and the two approaches, NTFA (red dashed line) and MTI (blue dotted line) models. (a): Test 1. (b) Test 2.

The following comments can be made:

1. Both approaches are in excellent agreement with the reference results. The NTFA model with 18 internal variables is as accurate as the MTI one with 30 internal variables, at least for predicting the effective response of the composite.

2. For NTFA model it is worth noting that although the modes have been generated from a set of snapshots corresponding to monotonic loading along specific directions, the NTFA model are still accurate for the more complex loadings of tests.

6.3 Average Fields of MTI and NTFA models

The average of the stress in the three different phases are compared in Figure 3. The norm of the average stress $\overline{\boldsymbol{\sigma}}^{(r)}$ in each constituent is used for this comparison:

$$\overline{\sigma}_{ij}^{(r)} = \frac{1}{V_r}\int_{V_r} \sigma_{ij}(\boldsymbol{x})\, d\boldsymbol{x}, \quad \left\|\overline{\boldsymbol{\sigma}}^{(r)}\right\| = \left(\sum_{i,j=1}^{3} \overline{\sigma}_{ij}^{(r)}\overline{\sigma}_{ij}^{(r)}\right)^{1/2}. \tag{22}$$

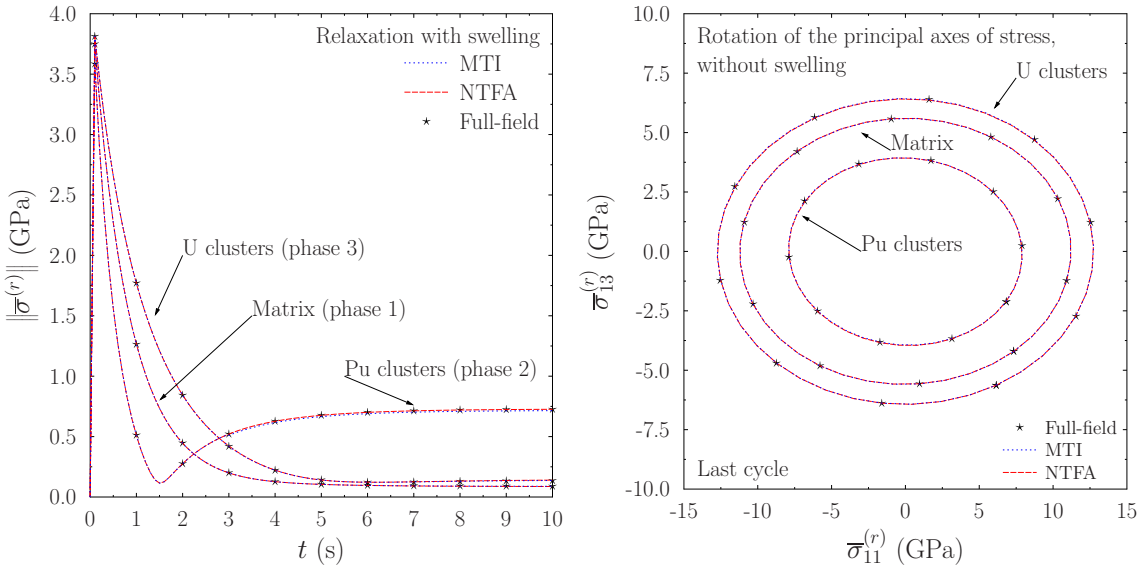

(a) (b)

Figure 3: Average response of the phases. Comparison between full-field simulations (black symbols), the two approaches NTFA (red dashed line) and MTI (blue dotted line) models. (a): Test 1. (b): Test 2. Last cycle.

The agreement of the two approaches with the reference results is again excellent. In test 1 (relaxation), both approaches are able to capture the quick relaxation of stress in the the Pu phase, followed by a progressive reloading of this phase, consequence of swelling and of the relaxation of the two other phases. In that particular situation, the *Hashin-Shtrikman* scheme used by MTI yields remarkably good predictions even for an inclusions volume fraction equal to 40%. This illustrates the fact that even though the overall loading is monotonic, the local response in the phases can be quite complex, a complexity that the MTI and NTFA models capture well. However, we can notice that the NTFA model yields slightly more accurate predictions than MTI in Pu Clusters. Finally as reported in [2] it's worth emphasizing that the NTFA predict also very well the field distribution in the volume element.

7 Conclusion and future works

In this study we compared two micromechanical approaches (MTI an analytical model and NTFA a reduced order model) of a three-phase particulate composite material with two inclusion phases dispersed in a contiguous matrix. The phases had a linear viscoelastic behavior with swelling. The theoretical comparison realized in this paper underlines a huge analogy between the two approaches. This point should facilitate the implementation of the NTFA method in Finite-Element Computation of fuel rods behavior under irradiation. The evolution laws enabling to compute the internal variables are similar: a system of differential equation of order one. Nevertheless, in the NTFA approach the internal variables are scalar and solve a system of coupled differential equations where the numerical coupled term isn't negligible. In the NTFA model the coefficients of these evolution laws are directly provided by full-field

computations while they are directly expressed as functions of the volume fraction of the phases as well as their elastic and viscous properties in the MTI one. The accuracies of both models were assessed by comparison with full-field simulations on different tests. The predictions (results for the overall response of the composite as well as for the average response of the phases) of both models are in excellent agreement with full-field simulations for various loading conditions. The NTFA model with 18 internal variables is as accurate as the MTI with 30 internal variables. In future works, it would be interesting to study if the relaxation times of MTI model would not be a new way to select the plastic modes of the NTFA approach. Moreover, it would be also interesting to compare NTFA and MTI models for a three-phase particulate composite material whose phases have a non linear viscoelastic behavior with swelling.

References

[1] Blanc V., Barbié L., Largenton R., Masson R., Homogenization of Linear Viscoelastic Three Phase Media: Internal Variable Formulation versus Full-field Computation. Int. Conf. Mech. Procedia 00 (2011) 1–6.

[2] Largenton R., Michel J.-C., Suquet P., Extension of the nonuniform transformation field analysis to linear viscoelastic composites in the presence of aging and swelling. Mechanics of Materials, 73 (2014) 76–100.

[3] Mandel, J., Cours de mécanique des milieux continus. Tomes I et II. Gauthier–Villars réédition (1994) J. Gabay.

[4] Michel J.-C., Moulinec H., Suquet P., Effective properties of composite materials with periodic microstructure: a computational approach. Comput. Methods Appl. Mech. Engrg., 172 (1999) 109–143.

[5] Michel J.-C., Suquet P., Nonuniform transformation field analysis. Int. J. Solids Structures, 40 (2003) 6937–6955.

[6] Ricaud J.-M., Masson R., Effective properties of linear viscoelastic heterogeneous media: Internal variables formulation and extension to ageing behaviours. Int. J. Solids Structures, 46 (2009) 1599–1606.